Scientific African 7 (2020) e00228

Contents lists available at ScienceDirect

Scientific African

journal homepage: www.elsevier.com/locate/sciaf

Estimation of planetary boundary layer height from radiosonde profiles over West Africa during the AMMA field campaign: Intercomparison of different methods

J.N.A. Aryee*, L.K. Amekudzi, K. Preko, W.A. Atiah, S.K. Danuor

Meteorology and Climate Science Unit, Department of Physics, Kwame Nkrumah University of Science and Technology, Kumasi, Ghana

ARTICLE INFO

Article history:
Received 21 January 2019
Revised 2 September 2019
Accepted 7 November 2019

Editor: Dr. B Gyampoh

Keywords:
AMMA
DACCIWA
Planetary boundary layer
West Africa
Radiosounding

ABSTRACT

Deducing realistic planetary boundary layer heights (PBLH) is crucial for weather, climate and air quality models, despite its equivocal nature. In this paper, a comparative assessment of seven PBLH estimation methods has been performed, with radiosonde profiles taken during the African Monsoon Multidisciplinary Analyses (AMMA) project campaign from June, 2006 to July, 2007 over 18 locations in West Africa. First, PBLH was identified from the radiosonde profiles as the location of minimum gradients in mixing ratio (q), relative humidity (RH) and refractivity (N), and maximum gradient in potential temperature (θ). Other methods used to identify PBL tops were the statistical NS method and bulk Richardson (Ri_b) method at a critical threshold of 0.25. Next, a reference method (h_o) was identified as the benchmark for PBL comparison. Visual inspection of the individual profiles allowed for assessing the h_o method to yield reliable PBLH estimates. Thereafter, comparisons of the PBLH were performed for both convective and stable cases, with the stable boundary layer (SBL) height being generally below 700 m a.g.l for all methods, whereas, convective boundary layer (CBL) heights ranged between 300 m a.g.l and 1400 m a.g.l across different regions of the study area. Contrarily, the NS method failed to detect the SBL due to its inability to identify a dewpoint or virtual potential temperature discontinuity. Additionally, the Ri_b method, particularly in stable cases, yielded PBL tops consistent with the reference method (h_o) whenever the NLLJ was clearly defined due to contribution of wind shear beneath the jet core to turbulent kinetic energy (TKE) production. Afterwards, the study domain was split into three zones and the performance of each method was assessed per each zone. Spatially, the CBL height was observed to grow thicker in the north-east direction over the dry, arid regions, where integral values of sensible heat rapidly converted by surface net radiation, has significant influence on the growth of CBL throughout daytime. Other likely reasons for this observation are advection, orography and mechanical turbulence production. However, a reversal was observed at night with the SBL being thinner in the dry, arid regions and rather relatively, higher in the coastal regions. Finally, the statistical assessment, coupled with visual inspection of the individual profiles, showed that the gradient methods (particularly N) outperformed the Ri_b and NS methods, yielding very low biases as well as, high and statistically significant correlation co-efficients. These results are useful for enhancing the performance of PBL models over the region. Possible limitations to the findings of this study are the different ascent times between the sites, as well as the number of ascents per site, which

* Corresponding author.
E-mail address: jeff.jay8845@gmail.com (J.N.A. Aryee).

https://doi.org/10.1016/j.sciaf.2019.e00228

have potential implications for the results. Further work, based on observations from the DACCIWA (Dynamics-aerosol-chemistry-cloud interactions in West Africa) field campaign, is currently ongoing to also fully substantiate the role of radiation and energy budgets in PBL development, while further assessing their significant effect on the performance of the PBL-detection methods.

1. Introduction

The planetary boundary layer (PBL) is the lowest region of the atmosphere, characterized by large-scale turbulent atmospheric flows [33] and exchanges between the atmosphere and earth surface [35,36]. Significant energy, momentum, and mass transfer between the earth surface and the atmosphere are confined within the PBL, which evolves diurnally, in response to radiation and energy balance. Complexities of the structure of the PBL are mostly linked with influences by local terrain and land surface features, as well as, synoptic and mesoscale weather situations [41]. Such complexities make the accurate determination of the planetary boundary layer height (hereafter termed as PBLH) quite problematic, despite its vast importance in weather, climate and air quality models [35].

Due to the equivocal nature of deducing realistic PBLHs, several researchers have employed various methods to estimate this variable. These include the detection of peaks in low-level winds [19,21], inversions in potential temperature [39], mixing ratio [35], relative humidity [35], refractivity [4], and the bulk Richardson number approach [38]. Other remote-sensing methods, such as the use of sodar [11] and observation of sharp gradients in backscatter profiles of lidar [9,12,20,28,37], have been extensively used to deduce the PBLH. These methods mostly delineate the aerosol-dense PBL from the clean, free-atmosphere [9,13,33]. Alternatively, [33] estimated the PBLH from statistical kurtosis and variance of dewpoint and virtual potential temperature differences.

Despite the ability of each of these methods to capture the PBLH, some disparities in their estimated heights exist [35]. A performance assessment is therefore very necessary to fully exploit the benefits and caveats of the various observational PBLH-estimation methods. Although PBLH performance assessments and reviews have been undertaken globally [23,27,35] and for specific regions such as the Tropics [4], United States [21,22,33,36], Europe [34,36], Northern and Southern Africa [2,25], and been observed that the PBLHs produced by the various methods vary in order of few hundreds of meters, such studies have yet to be fully exploited over West Africa. The major limitation is sparsity of upper air data from the West African domain to aid in the undertaking of such PBL-prognosis. Additionally, there is limited scope in understanding of coupled surface-boundary layer processes over West Africa, owing to the limited number of upper air observations over the domain coupled with the complex and heterogeneous surface structure of the domain. This paper therefore, makes use of upper air datasets retrieved during the African Monsoon Multidisciplinary Analyses (AMMA) field campaign over West Africa, in order to assess the performance of each method and also observe if the surface heterogeneities over the West African domain have any influence on the PBLHs, as well as, their estimation methods.

The objectives of this paper therefore, are to (i) comparatively assess the performance of seven PBLH estimation methods using the AMMA radiosonde data over West Africa, (ii) assess the spatial variations in PBLHs as captured by all seven methods and (iii) identify the possible role of surface features (topography and vegetation cover) in the performance of these methods. A brief description of the data and analysis method used has been provided in Section 2. Background climatology has also been provided in Section 3, with the results discussed in Section 4. A critical assessment of the performance of the various PBLH estimation methods is presented, with further highlight on the spatial variabilities of the various methods. Finally, conclusions are drawn in Section 5.

2. Data description and method of analysis

As part of the African Monsoon Multidisciplinary Analyses (AMMA) project which sought to improve understanding of the West African Monsoon system [31], a wide-network of instruments were deployed for daily atmospheric observations over the sub-region. Data for this paper were obtained from frequent radio-soundings performed over the sub-region (see Fig. 1), for periods ranging between 2005 and 2008, as shown in Table 1. Majority of the soundings were performed at 1200 UTC, followed by 0000 UTC, with relatively less proportions of soundings at 3-h intervals (see Fig. 2). Sounding measurements were performed with VAISALA sondes (RS80-A, RS92). Upper-air observation data retrieved from the soundings included pressure, temperature, humidity, wind speed and wind direction. GPS technology was used for high-quality wind speed and direction measurements by the sondes. Humidity measurements performed with VAISALA sondes were characterized by daytime dry bias and night-time moist bias, which were moderate for RS92 sondes but large for RS80-A sondes. The bias were corrected accordingly after being diagnosed via collocated GPS measurements. Moreover, in most of the study locations,

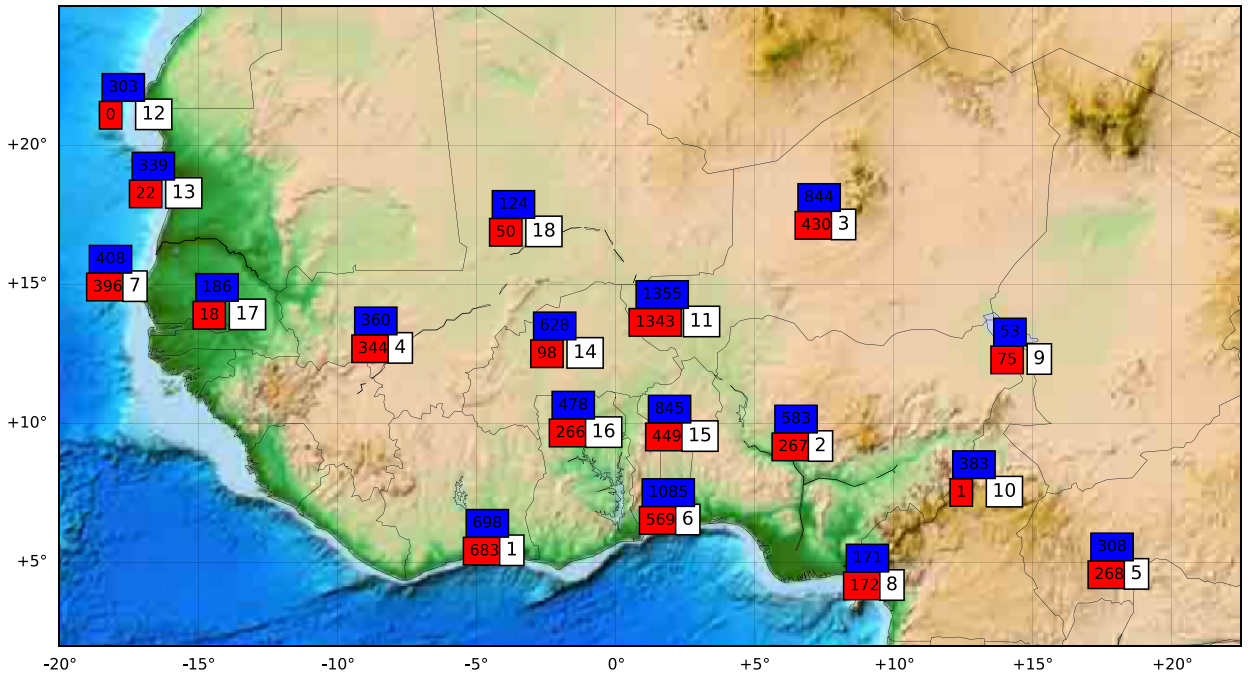

Fig. 1. Map of West Africa showing radiosonde launch points (white), with total number of nighttime (red) and daytime (blue) launches. (For interpretation of the references to color in this figure legend, the reader is referred to the web version of this article.)

Table 1
Summary of locations of AMMA radiosonde launch and duration of soundings from each station.

		Description			
Index	Station	Longitude	latitude	Elevation (m)	Total Obs. Period
1	Abidjan	−3.94	5.25	7	07/2006–12/2008
2	Abuja	7.16	9.00	370	06/2006–02/2008
3	Agadez	7.99	16.97	501	01/2006–08/2008
4	Bamako	−7.95	12.53	377	07/2006–07/2007
5	Bangui	18.52	4.40	395	04/2006–07/2007
6	Cotonou	2.39	6.36	135	06/2005–10/2008
7	Dakar	−17.49	14.75	28	11/2005–11/2007
8	Douala	9.73	4.00	5	03/2006–09/2006
9	N'Djamena	15.03	12.13	295	01/2006–10/2006
10	Ngaoundere	13.56	7.36	1104	02/2006–06/2007
11	Niamey	2.17	13.48	222	12/2005–12/2008
12	Nouadhibou	−17.03	20.93	8	04/2006–06/2007
13	Nouakchott	−15.95	18.10	3	04/2006–06/2007
14	Ougadougou	−1.52	12.35	310	02/2006–09/2008
15	Parakou	2.61	9.36	392	12/2005–10/2008
16	Tamale	−0.85	9.50	179	05/2006–10/2007
17	Tambacounda	−13.66	13.74	49	03/2006–10/2006
18	Tombouctou	−3.00	17.72	263	07/2006–11/2006

several variables were directly observed, however, some derivations were made for variables that were not directly observed. In order to apply similar PBLH-estimation schemes on the data from all stations, unobserved variables were deduced from Eqs. 1–4 by

$$T_d = \frac{c \times \log(\frac{RH}{100})\, e^{(b-\frac{T}{d})(\frac{T}{c+T})}}{b - \log(\frac{RH}{100})\, e^{(b-\frac{T}{d})(\frac{T}{c+T})}} \tag{1}$$

$$RH = \frac{q}{q_s} \times 100\% \tag{2}$$

$$u = -WS \sin\left(\frac{\pi}{180} WD\right) \tag{3}$$

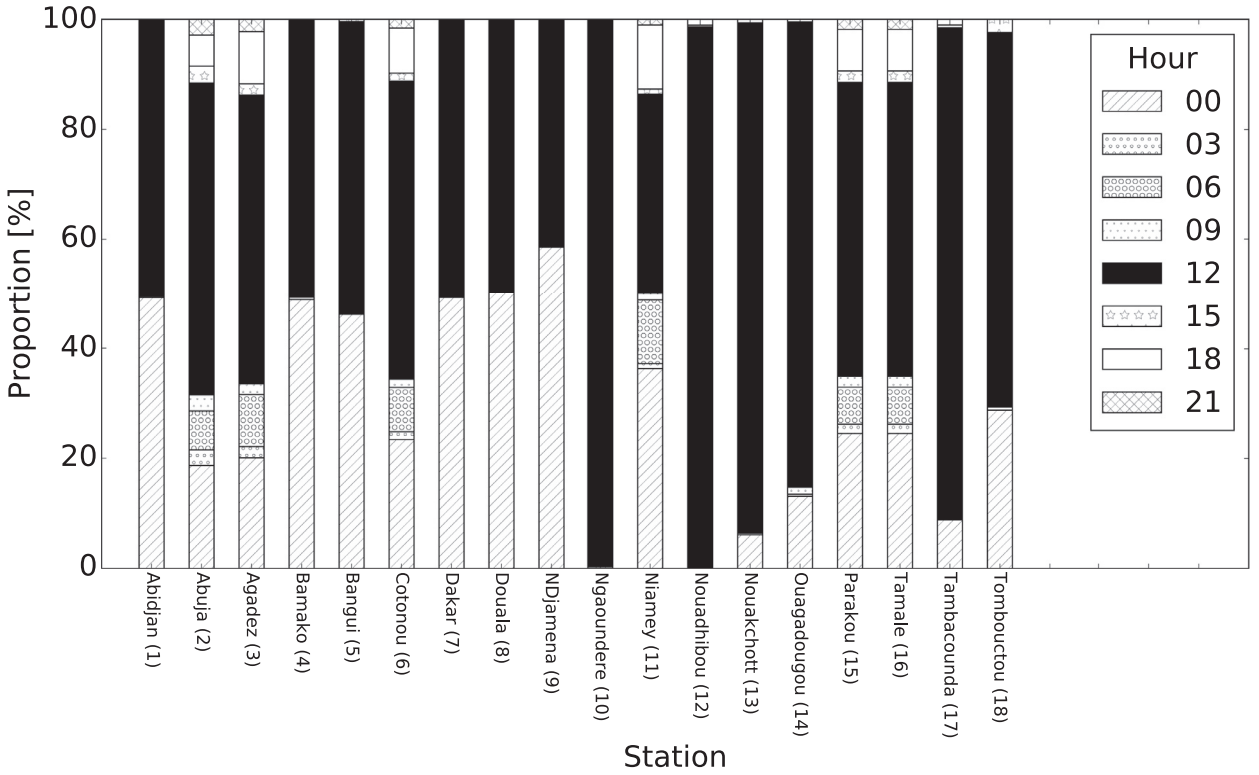

Fig. 2. Proportion of soundings performed at each location during the AMMA field campaign at 3 h intervals. Numbers in parenthesis correspond to radiosonde launch points in Fig. 1.

$$v = WS\cos\left(\frac{\pi}{180}WD\right), \tag{4}$$

where T_d is dewpoint temperature, T is air temperature, RH is relative humidity, q is mixing ratio, q_s is saturation mixing ratio, P is pressure, WS is wind speed, WD is wind direction, u is the zonal wind component, v is the meridional wind component, and b, c, and d are constants with typical values of 18.678, (238.88 for $T_d \leq$ 50; 247.15 for $T_d >$ 50), 234.50 respectively [6].

Table 1 provides geographic information on each station, with most of the locations being very low to mid-level lands, except Ngaoundere which is about 1.1 km above sea level (msl). In addition, the entire period of the upper air observation for each station has been provided in Table 1, however, for the purpose of this paper, datasets from June, 2006 to July, 2007 were used.

With uniform data structure, seven PBLH estimation methods were employed in detecting the top of the boundary layer, which included detection of maximum gradient in potential temperature (θ), minimum gradient in relative humidity (RH), minimum gradient in mixing ratio (q) and minimum gradient in refractivity (N). Alternative methods used were the detection of the index of bulk Richardson number (Ri_b) [see Eq. 5] [35], beyond the critical threshold [0.25 for this study, similar to [7,14,17,18]], and the NS method described in [33] [see Eqs. 6–10]. For the purposes of comparison, it was necessary to establish a reference method, hence the h_o method as described in [41] was selected as the reference method. The h_o method, first smoothens the gradient profiles and locates the 10 smallest gradients (largest for θ) of q, RH and N, with all 10 locations being possible PBL tops. Iterating through, from the smallest gradients (largest for θ), the first altitude where at least 3 of the four variables meet the criteria of PBLH simultaneously is marked as the PBLH. An error margin of 50 m is however allowed. The PBLH is termed missing if criteria is not met. For PBLH detection by all methods, a vertical limit of 3000 m a.g.l was set in order to avoid selecting mid-latitude inversions as PBL tops.

$$Ri_b = \frac{g}{\theta_{vo}}\frac{(\theta_{vz} - \theta_{vo})\,z}{u_z^2 + v_z^2}, \tag{5}$$

$$\sigma(x) = \frac{1}{N}\sum_{i=1}^{N}(x_i - \mu_x)^2, \tag{6}$$

$$\kappa(x) = \frac{\frac{1}{N}\sum_{i=1}^{N}(x_i - \mu_x)^4}{[\frac{1}{N}\sum_{i=1}^{N}(x_i - \mu_x)^2]^2} - 3, \tag{7}$$

$$S_i = |(d_1 - d_2)\,\sigma(d_3)\,\kappa(d_3)|, \tag{8}$$

$$\begin{aligned} d_1 &= \theta_v[(i-n):i] - T_d[(i-n):i] \\ d_2 &= \theta_v[i:(i+n)] - T_d[i:(i+n)] \\ d_3 &= \theta_v[(i-n):(i+n)] - T_d[(i-n):(i+n)] \\ |\theta_v(j+1) - \theta_v(j)| &> T_2, \end{aligned} \tag{9}$$

$$\frac{z(j+1) - z(j)}{|S(j+1)/S(j)|} > T_3, \tag{10}$$

where θ_v is the virtual potential temperature and T_d is the dewpoint at the surface (o) and other heights (z), σ is the variance, κ is the kurtosis, μ is the arithmetic mean and S is test statistic treating standard deviation and kurtosis as functions of a sample d_m (where m here ranges from 1 to 3). T_2 and T_3 were temperature and altitude thresholds, set at 0.5 K and 50 m, to test for θ_v-heterogeneity and strength of test statistic respectively.

According to Schmid and Niyogi [33], a challenge of the *NS* method is its inability to capture a dewpoint or θ_v discontinuity as delineation of the PBL top in most stable boundary layer profiles. Hence, the method performs best in the daytime convective boundary layer, unlike stable cases. Afterwards, an inter-comparison of the various methods was performed using various statistical metrics to include the Pearson's correlation co-efficient (r) at 95% and 99% confidence interval, bias, mean absolute error (MAE), root mean square error (RMSE), probability of detection (POD) and Nash–Sutcliffe efficiency (NSE), as described in [1,3,30]. These allowed for better assessment of each method's performance, relative to h_o. In order to avoid selecting very low PBLHs resulting from temperature inversions near the surface, all data below 50 m were excluded in deducing the convective boundary layer tops (although included in plots and SBL detection); a method similarly applied by [27,35,40] to remove noisy data near the ground.

All PBL methods were compared with standard PBL definitions, and the ones that conformed were used in further assessments. Also, PBL comparisons in this paper are made with respect to h_o, since it is dependent on best PBLH estimates of multiple methods (at least 3 gradient methods) agreeing on an identified PBLH with an error margin of 50 m. For brevity, the terms over-estimation and under-estimation are used in this paper with reference to the h_o-deduced PBLH.

3. Background climatology

The general tropospheric relative humidity, wind speed and wind direction profiles for three selected locations (Cotonou, Dakar and Niamey) have been examined, within the AMMA field campaign period (2006–2007). These sites were critically selected in order to evaluate the dynamics of annual atmospheric profiles and their spatial variabilities over widely-spaced regions of the study domain.

Fig. 3 shows the tropospheric wind profile for Cotonou (a,b), Dakar (d,e) and Niamey (g,h) for the 2006–2007 period, as well as, the humidity profile for Cotonou (c), Dakar (f) and Niamey (i). Notable features from these profiles are the African Easterly Jet (AEJ) and Tropical Easterly Jet (TEJ). For example, in Cotonou (see Figs. 3a and b), the AEJs were prevalent at 4 km [8,10], confirming the seasonality of AEJs in the tropics. Speed of AEJs ranged between 15 and 20 ms^{-1}. Notwithstanding, relatively few AEJs were discernible in Cotonou between July and September, as well as, December and March. Within the July – September months, winds at location of AEJs were now predominantly westerlies (see Fig. 3b). TEJs, on the other hand, were observed in Cotonou to be intensified within the monsoon season. Predominantly moist atmospheres existed all year especially at low levels (Fig. 3c), due to its location. Its atmospheric properties are impacted by the Atlantic Ocean. As expected, dry air intrusions are observed within the dry (harmattan) season spanning the month of January in the low-levels and November to March in the mid-troposphere.

Additionally, AEJs in Dakar (see Fig. 3d and e) were observed only within the monsoon season, with wind speeds between 15 m s^{-1} and 25 m s^{-1}. The dry periods were characterized by weak westerly winds. Similarly, the TEJs were observed to be monsoon occurrences with similar wind speeds as the AEJs. On the contrary, the dry periods in Dakar were characterized by strong, westerly upper tropospheric winds, which spanned the 8–16 km vertical extent (Fig. 3f). Also, the atmosphere was fairly humid. Atmospheric moisture increased either close to the surface or at mid-level (5–10 km) with *RH* ranging from 60% to 90%, especially within the Monsoon periods (June to early October). On the contrary, observations of dry air intrusions were observed in the core of the dry to pre-monsoon periods, which partitioned the surface and the mid level moisture. These dry air intrusions, as discussed in [24], limit the development of deep convection. The dry air intrusions from the dry to pre-monsoon periods, were observed to be somehow stronger in Niamey. An all-year intense moisture pattern existed in the mid-troposphere.

Furthermore, AEJ seasonality in Niamey was similar to Dakar, however with a slightly, wider vertical extent. These AEJs were again observed to be monsoon season-existent, with wind speeds on the order of 15–20 ms^{-1}. Speed of the AEJs

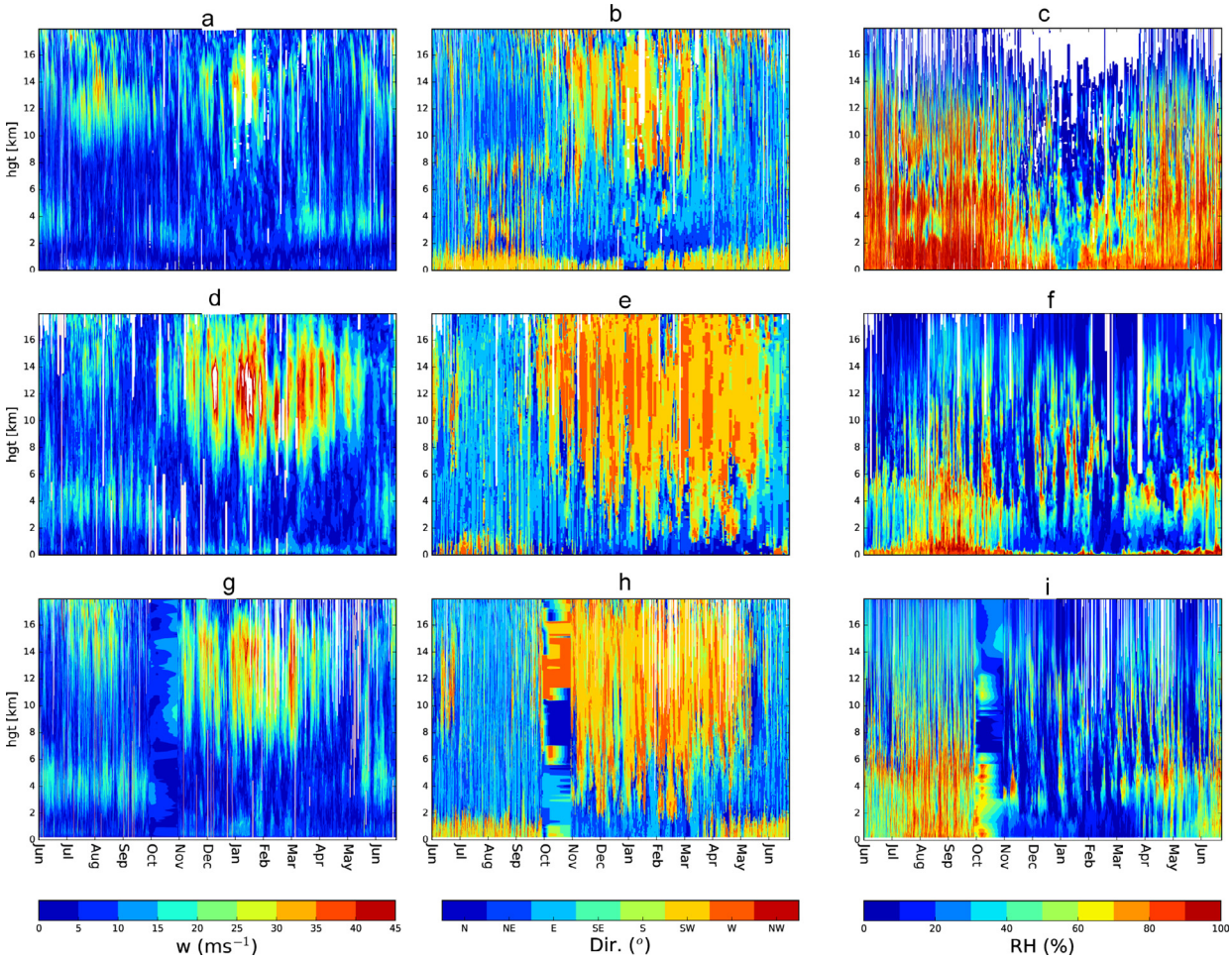

Fig. 3. Wind speed (left), wind direction (center) and relative humidity (right) profiles from Cotonou (a,b,c), Dakar (d,e,f) and Niamey(g,h,i) respectively.

were slightly lower than in Dakar, especially during the monsoon periods, which is similar to observations by Kante et al. [24]. The TEJs were again observed to be similar to that of Dakar, and particularly, existent during the monsoon periods, with speeds however slightly above Dakar. Upper tropospheric wind profiles in the dry periods were similar to Dakar, with prevailing strong, westerly winds observed between 8 and 16 km. However, these westerly winds were stronger in Dakar than in Niamey (see Fig. 3d and g).

In addition, Niamey was characterized by fairly moist low-to-mid levels within the monsoon periods and long-phased dry periods with vast (low, mid and upper tropospheric level) dry air intrusions during the dry/Harmattan season, extending from November to April (Fig. 3i).

4. Results and discussion

4.1. Estimation of the planetary boundary layer height (PBLH)

Fig. 4 shows the height of the convective boundary layer (CBL) from a 1200 UTC sounding performed in Niamey on July 23, 2006. Generally, the CBL height was detected by all methods, although there existed some variations in the height estimates identified by each method. This observation is due to the clearly-defined daytime delineation of the more dense boundary layer from the clear free-atmosphere [15,26]. The CBL is very turbulent and interactive with the earth's surface whereas the free-atmosphere is mostly stably-stratified or intermittently turbulent, and this allowed for all methods to detect the CBL top.

In all instances, the top of the CBL was clearly marked by a sharp vertical profile gradient, showing the abrupt change in atmospheric properties between the boundary layer and the free-atmosphere. Ri_b-detected PBL tops were, in most cases, marked by either a change in the direction of wind propagation (Fig. 4g) or a reduction in the magnitude of wind speed, or even both. Particularly in the monsoon periods, the CBL was capped by a region of backing vertical winds (see Fig. 4g), which

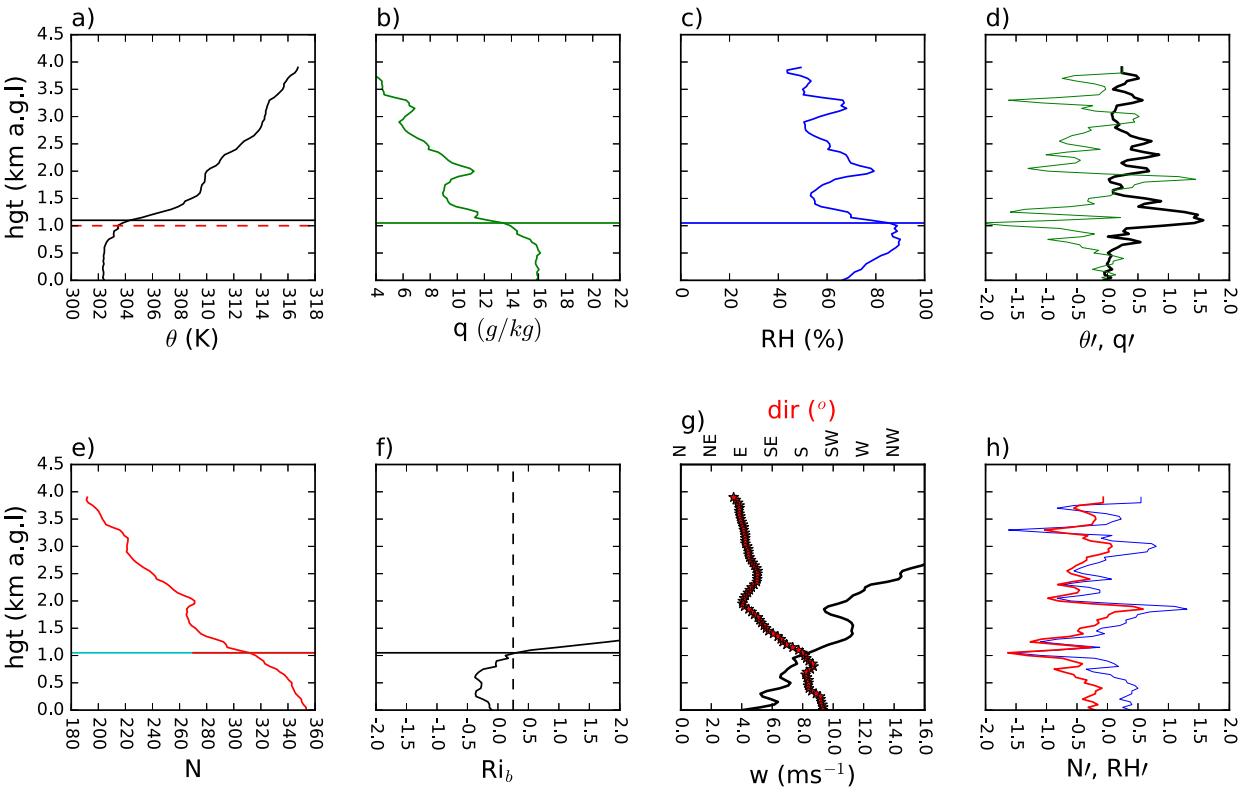

Fig. 4. Detection of convective boundary layer height from (**a**) potential temperature [θ-PBLH shown in black and *NS* in red], (**b**) *q*, (**c**) *RH*, (**e**) *N* [*N*-PBLH in red and h_o in cyan] and (**f**) Ri_b for 1200 UTC sounding taken on July 23, 2006 in Niamey. Vertical gradients of θ and *q* are provided in **d**, as well as, *N* and *RH* in **h**. Also, wind speed (black line) and direction (red star) have been provided in **g**. (For interpretation of the references to colour in this figure legend, the reader is referred to the web version of this article.)

are relatively stronger than the winds in the CBL. This is expected, since friction within the surface and complementing mixing in the PBL exerts a drag on the boundary layer winds. However, in the free-atmosphere where there is generally stratification of atmospheric properties, winds are expected to be stronger, due to the reduced impact of surface friction and mixing, which thus allows for the delineation of the CBL top by Ri_b.

Moreover, although not shown, the NS method was observed in most cases, to only mark the top of the fully mixed layer. This accounted for the relatively low CBL heights observed in most locations as provided in Fig. 6b. The other methods, particularly the gradient methods, were able to delineate the surface to the top of the capping inversion as the PBL top, unlike the NS method.

Fig. 5 shows the stable boundary layer profile from the ascent performed at 0000 UTC on September 20, 2006 in Niamey. The various methods yielded reliable stable boundary layer (SBL) heights, except the NS method. The NS method failed to identify dewpoint or virtual potential temperature discontinuities beyond potential SBL tops. The SBL height in Fig. 5 was approximately 200 m a.g.l for Ri_b and the moisture-based methods, whereas the temperature-method yielded SBL height of approximately 250 m a.g.l.

Intermittent turbulence, driven by the wind shear beneath the nocturnal low-level jet (NLLJ) core, is observed (see Fig. 5f and g). The NLLJ core marked the SBL top. Beneath the jet core, marginal mixing exists in the SBL, as evidenced by the nearly-uniform thermal and moisture structure in Fig. 5a, b and e. Similar to [5], however for periods when the NLLJ was clearly defined, the contribution of wind shear to the turbulent kinetic energy (TKE) production mostly yielded PBL tops which were consistent with the reference method (h_o).

4.2. Spatial fields assessment of planetary boundary layer heights

Sounding profiles at 0000 UTC and 1200 UTC were further assessed for all locations, except Ngaoundere and Nouadhibou, partly because most of the sites had substantial ascents at these hours. No 0000 UTC launches were made at Ngaoundere and Nouadhibou. The profiles at the two particular hours provide estimates of the stable and convective PBLHs.

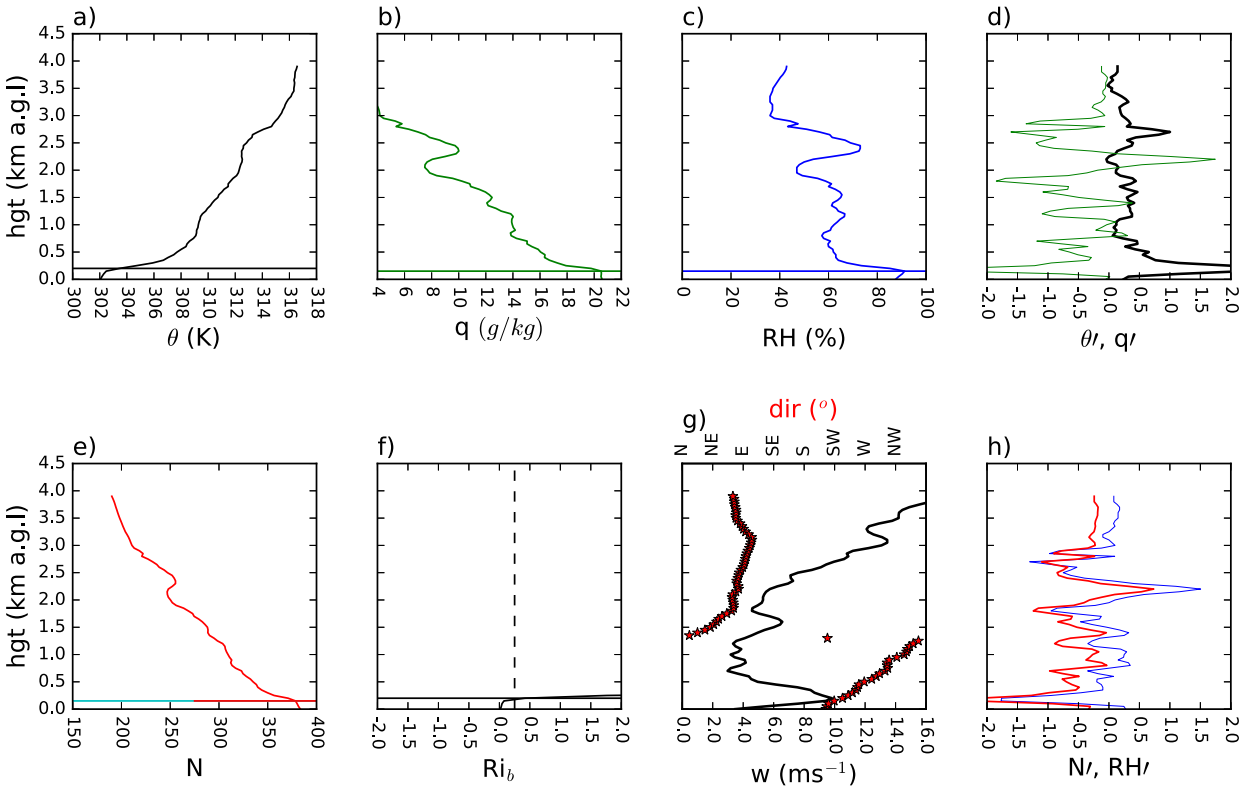

Fig. 5. Detection of stable boundary layer height for 0000 UTC sounding taken on 20th September 2006 from Niamey, with definitions as given in Fig. 4.

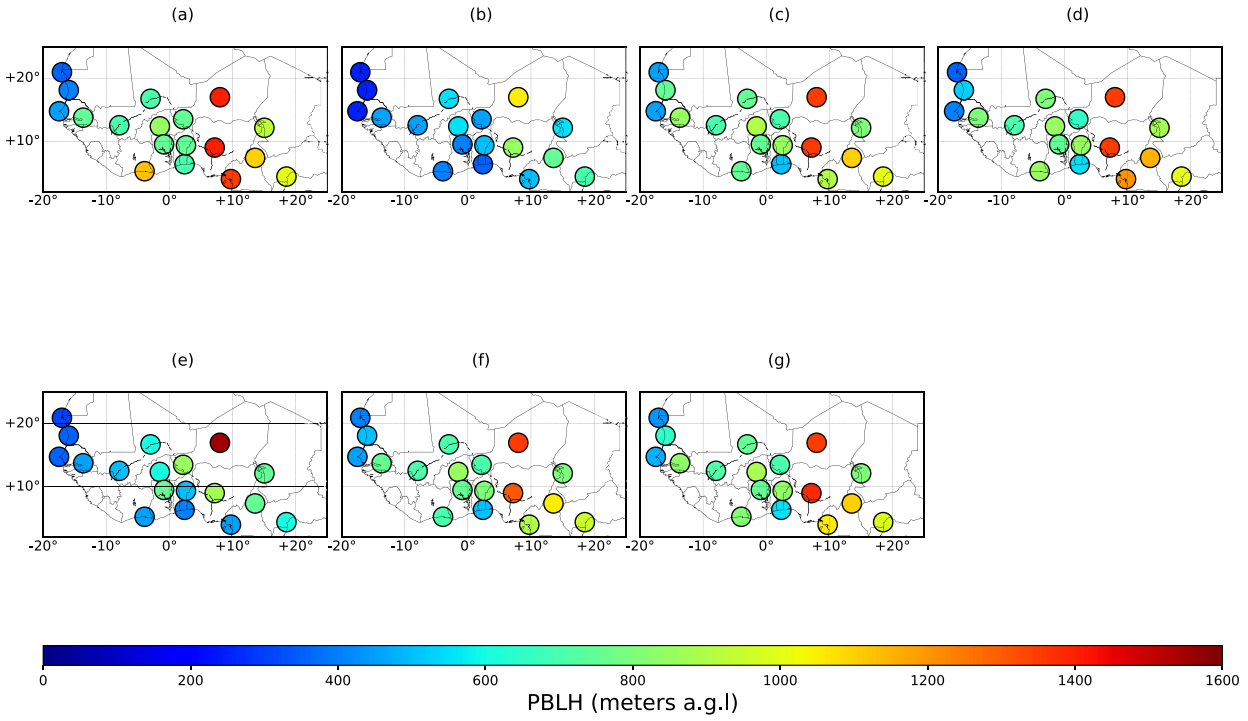

Fig. 6. Mean convective boundary layer height estimated from radiosonde profiles over all the stations by (a) θ- , (b) *NS*- , (c) q- , (d) *RH*- , (e) Ri_b- , (f) N- and (g) h_o- methods.

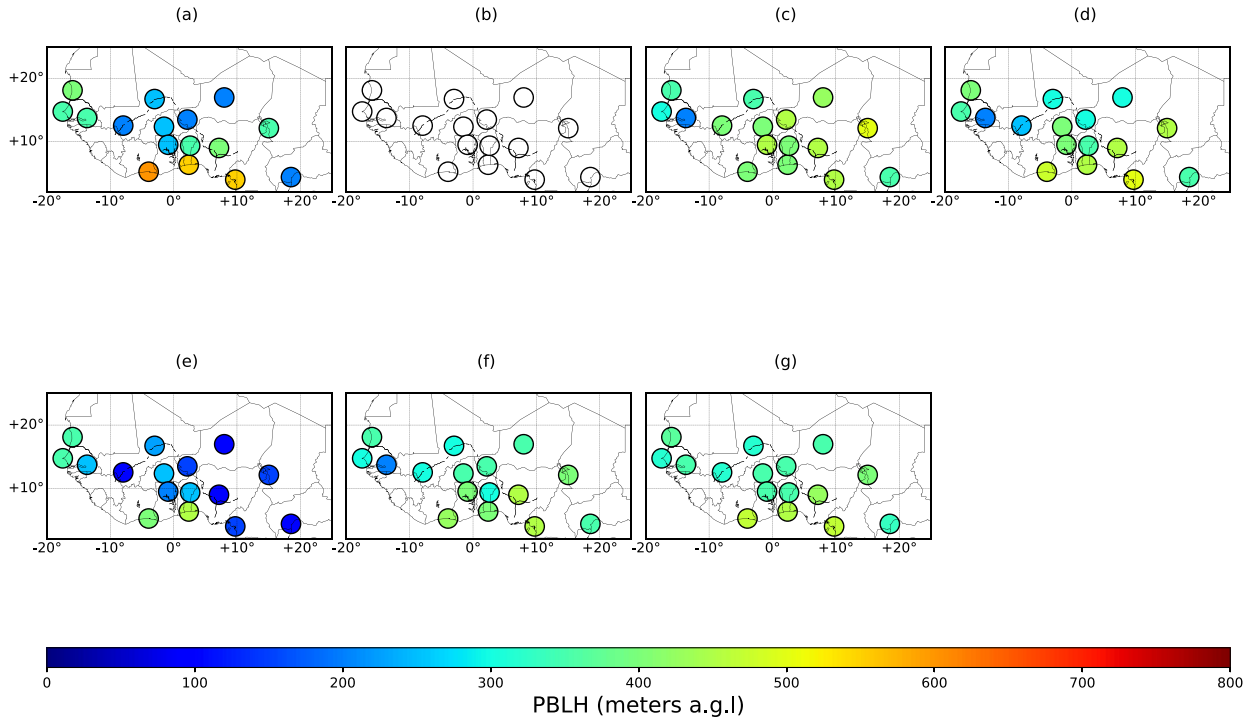

Fig. 7. Mean stable boundary layer height estimated from radiosonde profiles over all the stations by (a) θ- , (b) *NS*- , (c) *q*- , (d) *RH*- , (e) Ri_b- , (f) *N*- and (g) h_o- methods.

4.2.1. Mean convective boundary layer height

The CBL heights, estimated by each method for the individual stations, have been mapped in Fig. 6. In general, the CBL heights were observed to be lower in the north-western end of the study domain. These regions are dominated by relatively low-lying coasts and more vegetative cover, which thus impact on the extent of the CBL height. The sensible heat flux from this region is low, in comparison with the interior domains, due to the impact of moisture from the Atlantic. This likely accounts for the reduced PBLH development over these areas. As demonstrated by recent studies [32], the PBLH tends to shrink over moist terrains.

Also, the CBL heights were observed to grow thicker in the north-east direction, as captured by all the methods in Fig. 6. It is obvious from this observation that, the CBL heightens over dry, arid lands and is lowered over coastal lands [16,24,29]. According to Qiang and Sheng [29], in most arid areas, because of a lack of cloud-cover in the sky and the dry surface, strong solar radiation along with its significantly responsive thermodynamic process at the land surface are prominent factors in PBL formation and development.

Moreover, thermal developments in Abidjan showed a nearly-uniform warming pattern over wider vertical extents, which is evidenced by the higher PBLHs as shown in Fig. 6a, although the other methods yielded relatively low PBLHs. In all, the CBL heights were observed to range between 300 m a.g.l and 1600 m a.g.l. Consistently, *NS* underestimated the CBL heights in all locations, since in most cases, it only marked the top of the fully mixed layer and not the entire PBL (with the capping inversion inclusive). This occurs since the dewpoint and virtual temperature discontinuities begin from the top of the mixed layer. On the other hand, the Ri_b method, although underestimated for most locations, yielded very high CBL heights in Niamey, as compared to h_o.

4.2.2. Mean stable boundary layer height

Fig. 7 shows the mean SBL heights deduced by each method for the individual stations. No nighttime soundings were performed in Ngaoundere and Nouadhibou. Generally, the SBL heights were observed to be lower in the arid, northern to north-eastern ends of the region, whereas SBL heights in coastal regions were relatively higher. At night, the arid lands cool faster than the coastal surfaces. The surface inversions are thus pronounced and relatively lower in the arid regions, which culminates in the observed SBL structure.

In all, the SBL heights in the study region ranged approximately between 150 m a.g.l and 650 m a.g.l. Also, the *NS* method, as shown in Fig. 7b, failed to detect SBL tops for all stations and hence is not reliable for estimating SBL heights, which is consistent with observations of [33].

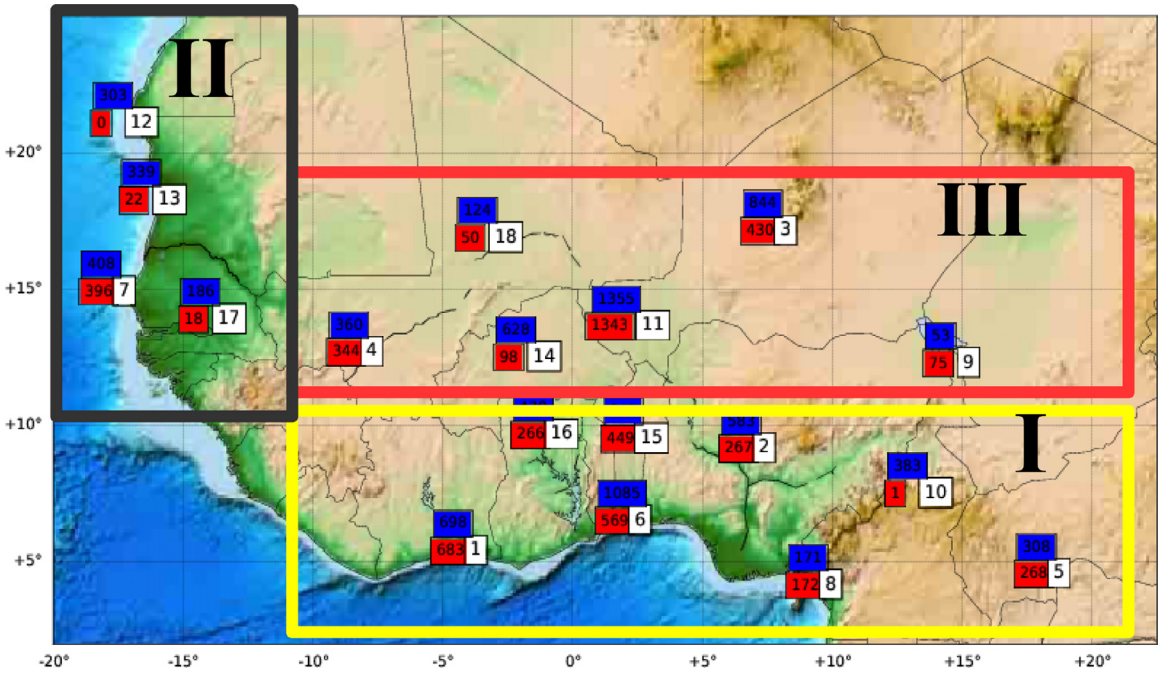

Fig. 8. Zonification of the study domain.

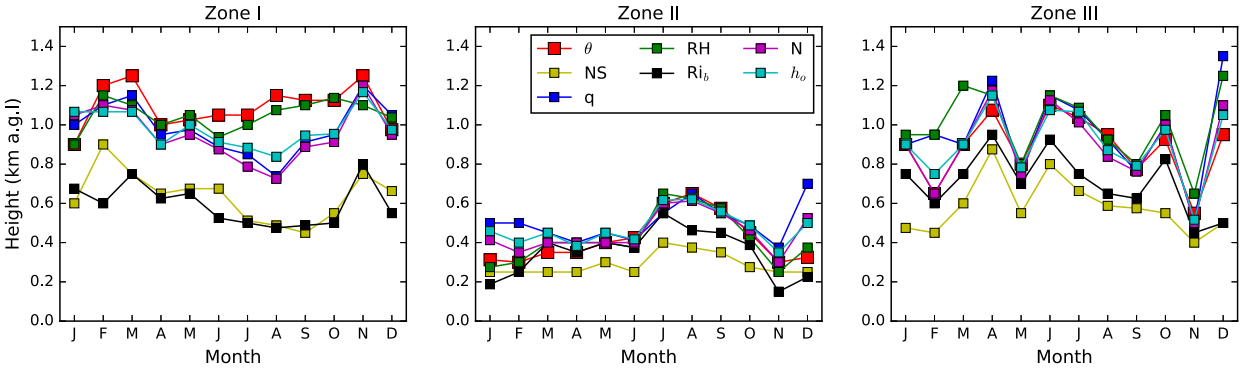

Fig. 9. Monthly pattern of CBL median heights from the three zones.

4.2.3. Zonified monthly mean PBLH

In order to analyse the influence of geographical location and topography to the PBL development, the study area was characterized into three zones, based on differences in topography and weather patterns Fig. 8. Zone I is the southern end of West Africa (latitude 3 °N – 10 °N, longitude 10 °W – 20 °E) which is covered with fairly adequate vegetation and is characterized mostly by bimodal rainfall patterns. Zone II is the western coast of West Africa (latitude 10 °N – 25 °N, longitude 20 °W – 10 °W), which is also covered by substantial vegetation, although characterized by a unimodal rainfall pattern. Zone III, on the other hand, is north of the first zone (latitude 10 °N – 20 °N, longitude 10 °W – 20 °E) and is characterized by vast arid lands with few highlands to its north-eastern end. The zone is also characterized by unimodal rainfall pattern, that lasts extremely short periods.

Fig. 9 shows the median, monthly evolution of CBL from the three delineated zones. In Zone 1, CBL heights were found to range between 0.7 km a.g.l to 1.3 km a.g.l. Contrarily, both *NS* and Ri_b underestimated the CBL tops by margins of 200–500 m. Similar seasonal patterns were observed by all the methods, with *RH* and θ however overestimating the CBL heights, particularly within the monsoon periods.

Zone 2, on the other hand, which was dominated by vegetative, coastal lands, yielded very low CBL heights. The CBL height estimates ranged between 0.2 km a.g.l and 0.7 km a.g.l. Nonetheless, all methods showed a similar seasonal pattern. Zone 3, which comprised of vast, dry, arid lands yielded very variable seasonal CBL heights. Their seasonal patterns, unlike the first two zones, were defined although by a first phase increment between January and April, followed by a decline in CBL height till November, and then an increase again in December.

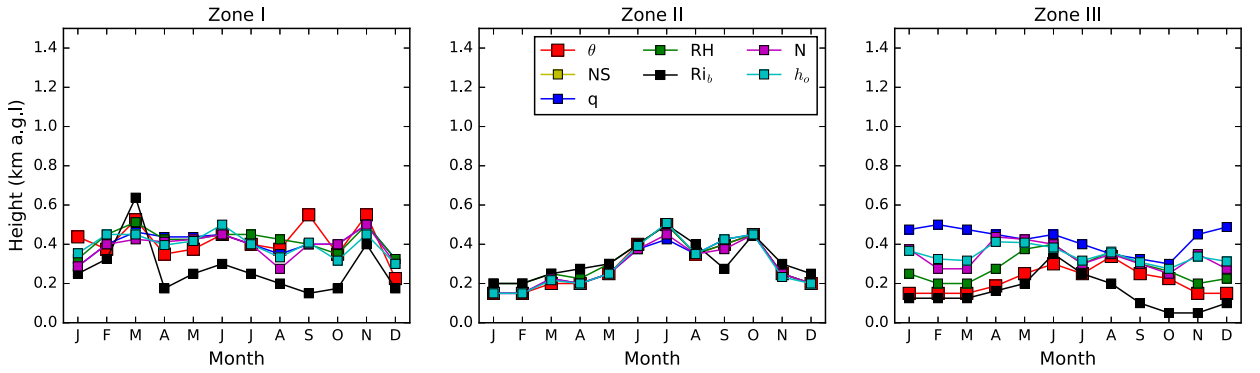

Fig. 10. Monthly pattern of SBL median heights from the three zones.

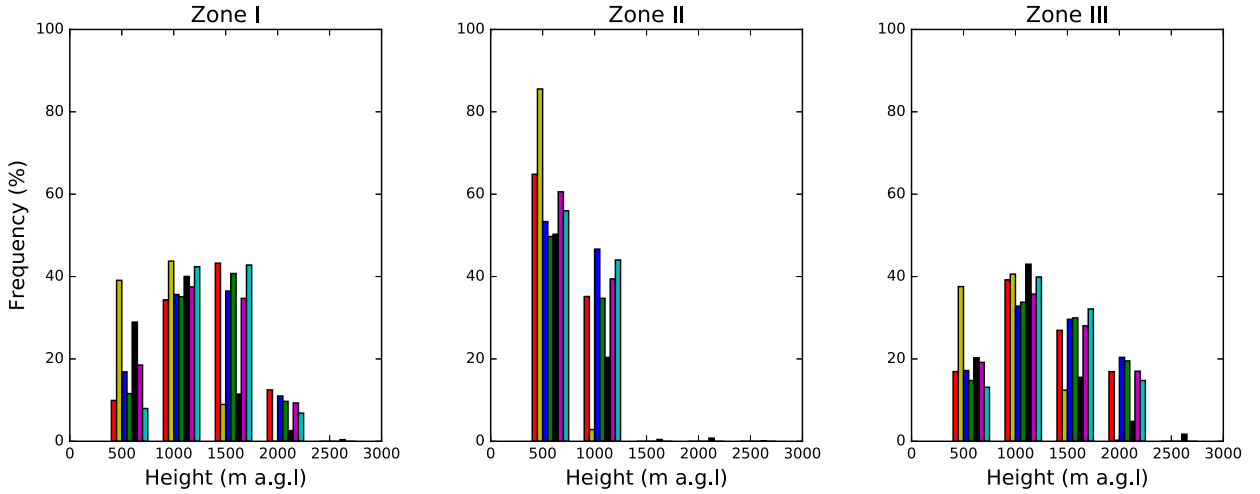

Fig. 11. Distribution of detected PBL heights in all zones. Labels are similar to Fig. 9.

In all, the various methods, for all zones mimicked the monthly patterns of h_o, although in some instances, over-estimations and under-estimations were recorded.

For stable cases, as shown in Fig. 10, the SBL heights were relatively reduced in all zones throughout the entire year, although larger reductions were observed over zones 1 and 3. Also, the monthly patterns by each method, were variable. Mean SBL heights ranged from approximately 0.2–0.6 m a.g.l, 0.2–0.5 m a.g.l and 0.15–0.5 m a.g.l in zones 1, 2 and 3 respectively. The various methods were consistent particularly in zone 2. However, in zones 1 and 3, the Ri_b method yielded relatively low estimates. *NS* method, on the other hand, failed at detecting a single SBL top, which confirms the unreliability of the method in SBL cases [33]. This occurrence is due to the inability of the method to observe dewpoint discontinuity or virtual potential temperature discontinuity beyond the potential PBL tops.

To better understand the distribution of identified PBL heights in each zone, the frequencies of 500 m height-binned PBL tops were assessed per zone (Fig. 11). In Zone 1, majority of the PBLHs were observed within the 1000 and 1500 m a.g.l range, followed by the very few 500 m a.g.l. Sparse PBL tops were detected within the 2000 m a.g.l bin. Zone 2, on the other hand, yielded majority of the PBL tops in the first 1000 m, with few Ri_b estimates ($\approx$ 1%) within the 1500 m and 2000 m a.g.l bin. These rather low PBL estimates, are attributable to the coastal and vegetative nature of the zone. The moist surface features tend to impact on the heat budgets, producing higher latent heat and lower sensible heat, culminating in reduced PBLHs, as demonstrated by Sanchez-Mejia [32]. In Zone 3, variable PBL tops were observed, ranging between the first 500 m to approximately 2000 m a.g.l. Majority of the height estimates, however, were between 1000 and 1500 m a.g.l, except the *NS* method which recorded high proportions between 500 m and 1000 m.

4.3. Statistical performance assessment

To assess the overall consistency and agreement between the various methods and the reference method (h_o), various statistical metrics were employed, as described in [1,3,30]. The statistics were performed per each zone, to observe if any significant differences existed per each individual terrain.

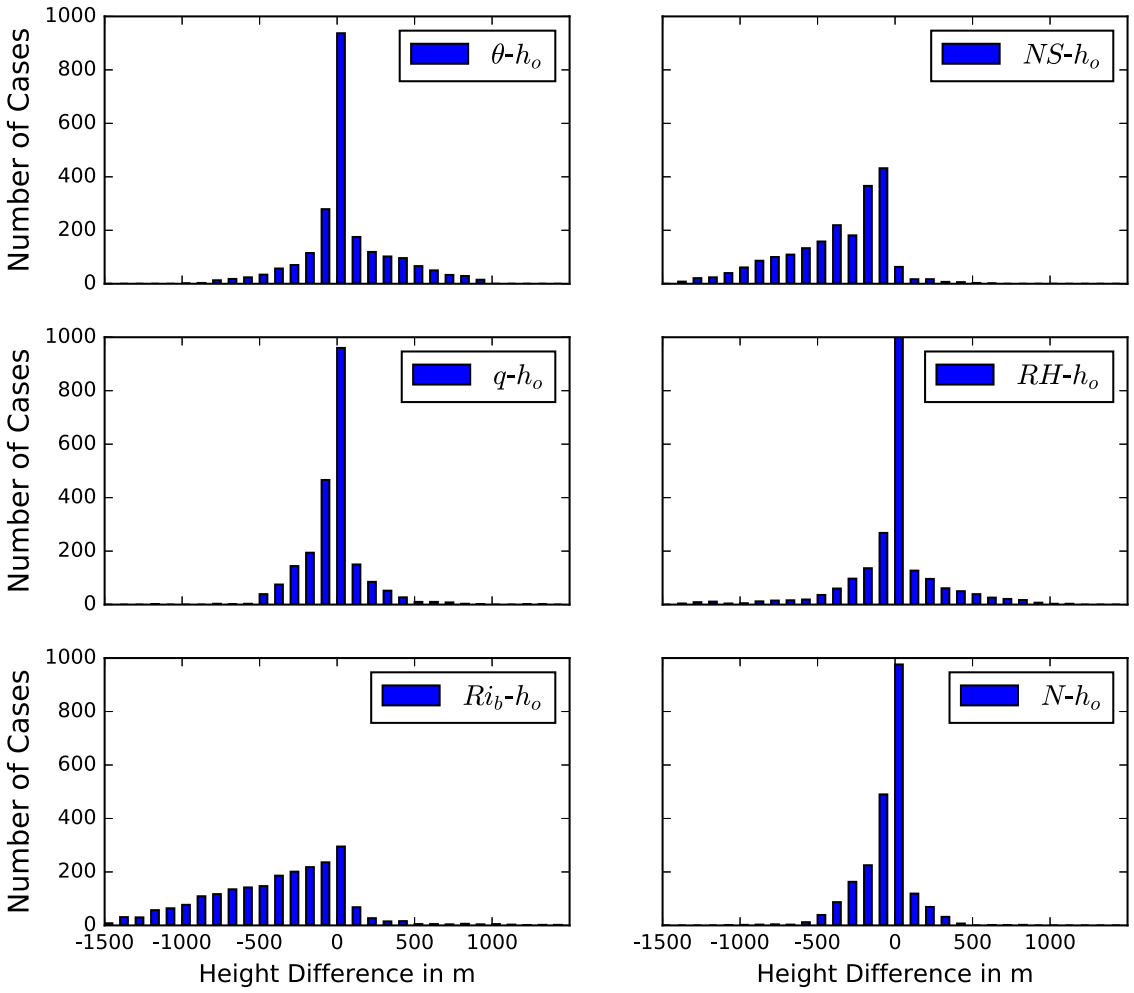

Fig. 12. Frequency distributions of differences between h_o and the other methods for all the PBL cases in Zone 1.

For Zone 1, bias between the various methods and h_o were of magnitudes of −63.28 m, −329.94 m, −13.60 m, 6.72 m, −359.08 m and −45.31 m for θ, *NS*, *q*, *RH*, Ri_b and *N* respectively (Table 2), with negatives representing underestimations and positives denoting overestimations. The bias statistics, coupled with the RMSE and MAE, reflect the underperformance of both *NS* and Ri_b, in matching the CBL heights detected by h_o. On the contrary, although *RH* recorded least overestimations than all the other gradient methods, the correlation analysis, NSE and the Probability of Detection show the relatively better performance of the *N* method than the other alternatives.

Similar observations were made in both zones 2 and 3, where statistically significant and higher correlation co-efficients of *N* confirms the performance of *N*, relative to the other alternatives. Moreover, error assessments in both zones 2 and 3 reveal a very low error margin between *N* and h_o, than the other methods. On the contrary, Ri_b and *NS* showed large underestimations of h_o.

Similarly, for SBL, error assessments and correlation analyses were performed and these again showed the *N* method to outperform the other alternatives, with high and statistically significant correlation co-efficients. These are also buttressed by very low bias values, which were on order of −11.52 m, −9.61 m and 10.86 m for zones 1, 2 and 3 respectively. Again, Ri_b seemed to largely differ from the h_o method, with bias values of −124.59 m, 14.59 m and −140.51 m, as well as, correlation co-efficients below 0.2 for zones 1, 2 and 3. *NS* was omitted from the SBL statistical assessments since it failed to detect a single SBL, which confirms the assertion of [33].

For both stable and convective cases, and based on further visual inspection of each individual profile, the gradient methods were found to outperform the *NS* and Ri_b methods. Moreover, the *N* method yielded good agreement with h_o and tends to outperform the other alternatives, which is consistent with observations of [4].

Next, comparisons of both SBL and CBL height estimates resulting from application of the different methods were made. Frequency distributions of the differences between h_o and the other characteristic heights are plotted in Figs. 12–14. Residual assessments were jointly performed for both stable and convective boundary layer types.

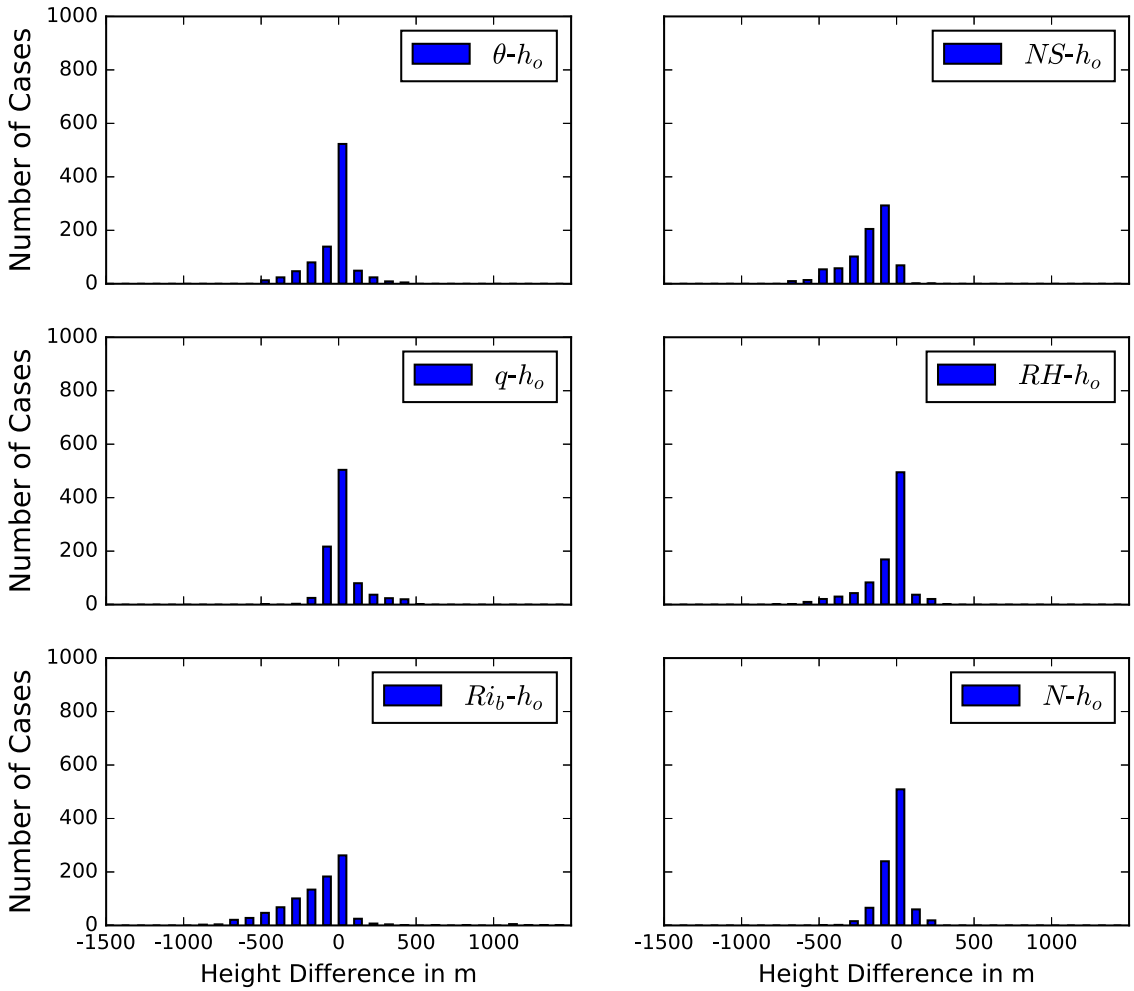

Fig. 13. Frequency distributions of differences between h_o and the other methods for all the PBL cases in Zone 2.

Table 2
Statistical metrices for CBL performance assessment of each method against h_o. Double astericks denotes significance at both 95% and 99% confidene level.

Zone	Method	Bias (m)	RMSE	MAE	P.O.D	NSE	r
I	θ	63.28	282.81	175.89	0.57	0.31	0.71**
	NS	−329.94	485.46	343.73	0.24	−0.88	0.43**
	q	−13.60	184.87	109.64	0.65	0.70	0.89**
	RH	6.72	289.30	167.22	0.62	0.27	0.70**
	Ri_b	−359.08	582.47	437.76	0.25	−1.94	0.30**
	N	−45.31	168.73	100.54	0.66	0.75	0.92**
II	θ	−24.90	130.82	76.63	0.74	0.54	0.81**
	NS	−154.45	229.69	155.40	0.45	−0.24	0.49**
	q	31.78	114.79	61.14	0.81	0.65	0.87**
	RH	−42.92	148.55	88.08	0.74	0.41	0.77**
	Ri_b	−115.04	312.75	189.67	0.51	−1.58	0.36**
	N	−6.44	79.98	46.31	0.83	0.83	0.93**
III	θ	−14.93	272.33	150.19	0.66	0.58	0.81**
	NS	−297.25	464.51	305.86	0.30	−0.11	0.61**
	q	38.36	200.47	99.99	0.72	0.77	0.91**
	RH	28.04	269.44	140.39	0.69	0.59	0.83**
	Ri_b	−218.68	554.55	362.75	0.37	−0.71	0.47**
	N	−13.98	165.96	88.18	0.73	0.84	0.94**

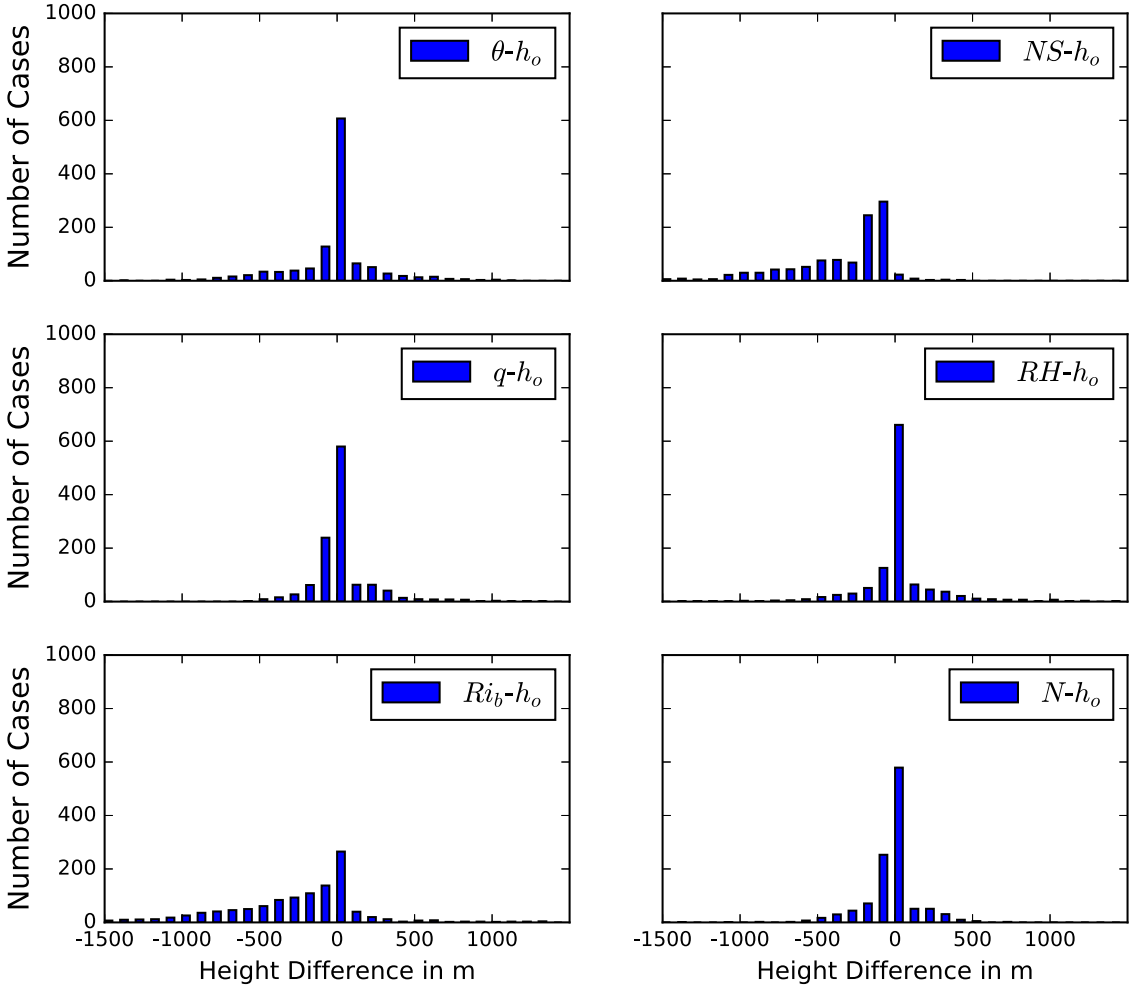

Fig. 14. Frequency distributions of differences between h_o and the other methods for all the PBL cases in Zone 3.

Table 3
Statistical metrices for SBL performance assessment of each method against h_o. Definitions same as Table 2.

Zone	Method	Bias (m)	RMSE	MAE	P.O.D	NSE	r
I	θ	10.67	154.34	105.52	0.64	0.09	0.70**
	NS	n/a	n/a	n/a	n/a	n/a	n/a
	q	0.09	92.86	62.11	0.77	0.67	0.87**
	RH	12.30	116.51	79.94	0.75	0.48	0.76**
	Ri_b	−124.59	318.53	214.34	0.39	−2.84	0.16**
	N	−11.52	84.72	56.84	0.79	0.73	0.90**
II	θ	14.66	92.30	43.43	0.87	0.70	0.88**
	NS	n/a	n/a	n/a	n/a	n/a	n/a
	q	−7.12	57.88	25.66	0.92	0.88	0.94**
	RH	10.10	67.82	41.77	0.93	0.84	0.92**
	Ri_b	14.59	340.91	154.29	0.64	−3.01	0.19**
	N	−9.61	47.52	22.34	0.93	0.92	0.96**
III	θ	−78.96	164.53	113.10	0.60	−0.08	0.64**
	NS	n/a	n/a	n/a	n/a	n/a	n/a
	q	60.05	127.72	82.24	0.69	0.35	0.83**
	RH	−20.09	137.38	97.30	0.67	0.24	0.65**
	Ri_b	−140.51	318.42	223.18	0.34	−3.02	0.16**
	N	10.86	95.68	64.79	0.74	0.63	0.88**

In Fig. 12, the residual of the gradient methods show a rather normal distribution, with peaks at 0 and majority of the deviations between ± 500 m of h_o. Deviations of both *NS* and Ri_b, however, are skewed in the negatives, which confirms the underestimations of h_o by both methods as observed in Tables 2 and 3.

Similarly, in Zone 2, the deviations of the gradient method showed a normal distribution with a range between ± 500 m. Again, the *NS* and Ri_b methods were skewed towards the negative, which again details the underestimation of the PBL (SBL and CBL) height by both methods.

Moreover, Zone 3 also showed similar distribution for the difference of the various methods with respect to h_o. It can be observed that the deviations of h_o and the gradient methods are within ± 500 m for the majority of cases, whereas, *NS* and Ri_b again are skewed towards the negative difference.

5. Conclusion

The performance of seven planetary boundary layer height estimation methods (θ, NS, q, RH, Ri_b, N and h_o) have been evaluated in this paper, using the AMMA radiosonde network data over West Africa, covering the period of June, 2006 to July, 2007.

First, a reference method (h_o) was identified as the benchmark for PBL comparison. The h_o method, first smoothens the gradient profiles and locates the 10 smallest gradients (largest for θ) of q, RH and N, with all 10 locations being possible PBL tops. Iterating through, from the smallest gradients (largest for θ), the first altitude where at least 3 of the four variables meet the criteria of PBLH simultaneously, with an error margin of 50 m allowed, is marked as the PBLH. Visual inspections of the individual profiles allowed for assessing the h_o method to yield reliable PBLH estimates. Thereafter, comparisons of the PBL heights were performed for both convective and stable cases. From the analysis, SBL heights were observed to be generally below 700 m a.g.l for all methods, whereas, CBL heights ranged between 300 m a.g.l and 1400 m a.g.l. The NS method failed to detect the SBL due to its inability to identify a dewpoint or virtual potential temperature discontinuity as delineation of the PBL top, which is consistent with the research findings of [33]. Also, with regards to the performance of the Ri_b method, particularly in stable cases whenever the NLLJ was clearly defined, the contribution of wind shear to the turbulent kinetic energy (TKE) production mostly yielded PBL tops which were consistent with the reference method (h_o).

Afterwards, the study domain was split into three zones and the methods were assessed in each zone. Spatially, the PBL heights were observed to grow in the north-east direction over the study domain. The findings of this study, support the argument that the CBL height thickens over the dry, arid regions, where integral values of sensible heat rapidly converted by surface net radiation, has significant influence on the growth of CBL throughout daytime [29]. Other likely reasons for this observation are advection, orography and mechanical turbulence production. However, at night, the SBL is thinner in the dry, arid regions and rather relatively higher in the coastal regions. Furthermore, the statistical assessment, coupled with visual inspection of the individual profiles, showed that the gradient methods outperformed both the Ri_b and *NS* methods. Precisely, the *N* method outperformed all the various methods, yielding very low biases as well as, high and statistically significant correlation coefficients. This, as detailed in literature, is due to its inclusion of both the temperature and moisture profiles. As such, it has the ability to detect even marginal vertical gradients from either the temperature or moisture profile.

The findings of this study are useful for enhancing the performance of PBL models over the region. Possible limitations to the findings of this study are the different ascent times between the sites, as well the number of ascents per site, which have potential implications for the results. Further work (Dynamics-aerosol-chemistry-cloud interactions in West Africa [DACCIWA] project) is currently ongoing to also substantiate the role of the radiation and energy budgets in PBL development over the study region, while further assessing if they have significant influence on the performance of each of these PBL detection methods.

Declaration of Competing Interest

The authors declare that they have no conflict of interest.

CRediT authorship contribution statement

J.N.A. Aryee: Conceptualization, Data curation, Writing - original draft. **L.K. Amekudzi:** Conceptualization, Data curation, Writing - original draft. **W.A. Atiah:** Validation. **S.K. Danuor:** Validation.

Acknowledgments

The authors have received funding from the European Union 7th Framework Programme (FP7/2007-2013) under grant agreement 603502 (EU project DACCIWA: Dynamics-aerosol-chemistry-cloud interactions in West Africa). The AMMA radiosonde data were obtained from the AMMA database at http://database.amma-international, a programme funded by the EU/FP6 AMMA project (Grant 004089). The authors also appreciate the KNUST for its institutional support.

References

[1] L.K. Amekudzi, M.A. Osei, W.A. Atiah, J.N.A. Aryee, M.A. Ahiataku, E. Quansah, K. Preko, S.K. Danuor, A.H. Fink, Validation of TRMM and FEWS satellite rainfall estimates with rain gauge measurement over ashanti region, ghana, Atmos. Clim. Sci. 6 (04) (2016) 500.
[2] C.O. Ao, D.E. Waliser, S.K. Chan, J.-L. Li, B. Tian, F. Xie, A.J. Mannucci, Planetary boundary layer heights from GPS radio occultation refractivity and humidity profiles, J. Geophys. Res. Atmos. 117 (D16) (2012).
[3] J. Aryee, L. Amekudzi, W. Atiah, M. Osei, E. Agyapong, Overview of surface to near-surface atmospheric profiles over selected domain during the QWeci project, Meteorol. Atmos. Phys. 131 (4) (2019) 1067–1081.
[4] G. Basha, M.V. Ratnam, Identification of atmospheric boundary layer height over a tropical station using high-resolution radiosonde refractivity profiles: comparison with GPS radio occultation measurements, J. Geophys. Res. Atmos. 114 (D16) (2009).
[5] F. Beyrich, J.-P. Leps, An operational mixing height data set from routine radiosoundings at lindenberg: methodology, Meteorol. Z. 21 (4) (2012) 337–348.
[6] A.L. Buck, New equations for computing vapor pressure and enhancement factor, J. Appl. Meteorol. 20 (12) (1981) 1527–1532.
[7] J.A. Businger, J.C. Wyngaard, Y. Izumi, E.F. Bradley, Flux-profile relationships in the atmospheric surface layer, J. Atmos. Sci. 28 (2) (1971) 181–189.
[8] K.H. Cook, Generation of the african easterly jet and its role in determining west african precipitation, J. Clim. 12 (5) (1999) 1165–1184.
[9] D. Cooper, W. Eichinger, Structure of the atmosphere in an urban planetary boundary layer from lidar and radiosonde observations, J. Geophys. Res. Atmos. 99 (D11) (1994) 22937–22948.
[10] A.K. Dezfuli, S.E. Nicholson, A note on long-term variations of the african easterly jet, Int. J. Climatol. 31 (13) (2011) 2049–2054.
[11] S. Emeis, C. Münkel, S. Vogt, W.J. Müller, K. Schäfer, Atmospheric boundary-layer structure from simultaneous SODAR, RASS, and ceilometer measurements, Atmos. Environ. 38 (2) (2004) 273–286.
[12] N. Eresmaa, A. Karppinen, S. Joffre, J. Räsänen, H. Talvitie, Mixing height determination by ceilometer, Atmos. Chem. Phys. 6 (6) (2006) 1485–1493.
[13] T. Gal-Chen, M. Xu, W.L. Eberhard, Estimations of atmospheric boundary layer fluxes and other turbulence parameters from doppler lidar data, J. Geophys. Res. Atmos. 97 (D17) (1992) 18409–18423.
[14] B. Galperin, S. Sukoriansky, P.S. Anderson, On the critical richardson number in stably stratified turbulence, Atmos. Sci. Lett. 8 (3) (2007) 65–69.
[15] J.R. Garratt, The atmospheric boundary layer, Earth Sci. Rev. 37 (1–2) (1994) 89–134.
[16] J.R. Garratt, G.D. Hess, W.L. Physick, P. Bougeault, The atmospheric boundary layer – advances in knowledge and application, Boundary-Layer Meteorol. 78 (1996) 9–37.
[17] A.A. Grachev, E.L. Andreas, C.W. Fairall, P.S. Guest, P.O.G. Persson, Outlier problem in evaluating similarity functions in the stable atmospheric boundary layer, Boundary-Layer Meteorol. 144 (2) (2012) 137–155.
[18] A.A. Grachev, E.L. Andreas, C.W. Fairall, P.S. Guest, P.O.G. Persson, The critical richardson number and limits of applicability of local similarity theory in the stable boundary layer, Boundary-Layer Meteorol. 147 (1) (2013) 51–82.
[19] R.L. Grossman, N. Gamage, Moisture flux and mixing processes in the daytime continental convective boundary layer, J. Geophys. Res. Atmos. 100 (D12) (1995) 25665–25674.
[20] M. Haeffelin, F. Angelini, Y. Morille, G. Martucci, S. Frey, G. Gobbi, S. Lolli, C. O'dowd, L. Sauvage, I. Xueref-Rémy, et al., Evaluation of mixing-height retrievals from automatic profiling lidars and ceilometers in view of future integrated networks in europe, Boundary-Layer Meteorol. 143 (1) (2012) 49–75.
[21] G.C. Holzworth, Estimates of mean maximum mixing depths in the contiguous united states, Mon. Weather Rev. 92 (5) (1964) 235–242.
[22] G.C. Holzworth, Mixing depths, wind speeds and air pollution potential for selected locations in the united states, J. Appl. Meteorol. 6 (6) (1967) 1039–1044.
[23] N.S. Jordan, R.M. Hoff, J.T. Bacmeister, Validation of goddard earth observing system-version 5 merra planetary boundary layer heights using calipso, J. Geophys. Res. Atmos. 115 (D24) (2010).
[24] I.K. Kante, D. Badiane, S.M. Sall, A. Deme, A. Diedhiou, Comparative study of the west african continental, coastal, and marine atmospheric profiles during the summer of 2006, Int. J. Geophys. 2012 (2012).
[25] K. Korhonen, E. Giannakaki, T. Mielonen, A. Pfüller, L. Laakso, V. Vakkari, H. Baars, R. Engelmann, J. Beukes, P. Van Zyl, et al., Atmospheric boundary layer top height in south africa: measurements with lidar and radiosonde compared to 3 atmospheric models, Atmos. Chem. Phys. 14 (8) (2014) 4263–4278.
[26] A. Lammert, J. Bösenberg, Determination of the convective boundary-layer height with laser remote sensing, Boundary-Layer Meteorol. 119 (1) (2006) 159–170.
[27] S. Liu, X.-Z. Liang, Observed diurnal cycle climatology of planetary boundary layer height, J. Clim. 23 (21) (2010) 5790–5809.
[28] C. Münkel, N. Eresmaa, J. Räsänen, A. Karppinen, Retrieval of mixing height and dust concentration with lidar ceilometer, Boundary-Layer Meteorol. 124 (1) (2007) 117–128.
[29] Z. Qiang, W. Sheng, A study of the atmospheric boundary layer structure during a clear day in the arid region of northwest china, J. Meteorol. Res. 23 (3) (2009) 327–337.
[30] E. Quansah, L.K. Amekudzi, K. Preko, J. Aryee, R.O. Boakye, D. Boli, M.R. Salifu, Empirical models for estimating global solar radiation over the ashanti region of ghana, J. Sol. Energy 2014 (2014).
[31] J.-L. Redelsperger, C.D. Thorncroft, A. Diedhiou, T. Lebel, et al., African monsoon multidisciplinary analysis: an international research project and field campaign, Bull. Am. Meteorol. Soc. 87 (12) (2006) 1739.
[32] Z.M. Sanchez-Mejia, Monsoon Dependent Ecosystems: Implications of the Vertical Distribution of Soil Moisture on Land Surface-Atmosphere Interactions, The University of Arizona, 2013 Ph.D. thesis.
[33] P. Schmid, D. Niyogi, A method for estimating planetary boundary layer heights and its application over the ARM southern great plains site, J. Atmos. Ocean Technol. 29 (3) (2012) 316–322.
[34] P. Seibert, F. Beyrich, S.-E. Gryning, S. Joffre, A. Rasmussen, P. Tercier, Review and intercomparison of operational methods for the determination of the mixing height, Atmos. Environ. 34 (7) (2000) 1001–1027.
[35] D.J. Seidel, C.O. Ao, K. Li, Estimating climatological planetary boundary layer heights from radiosonde observations: comparison of methods and uncertainty analysis, J. Geophys. Res. Atmos. 115 (D16) (2010).
[36] D.J. Seidel, Y. Zhang, A. Beljaars, J.-C. Golaz, A.R. Jacobson, B. Medeiros, Climatology of the planetary boundary layer over the continental United States and Europe, J. Geophys. Res. Atmos. 117 (D17) (2012).
[37] D.G. Steyn, M. Baldi, R. Hoff, Detection of Mixed Layer Depth and Entrainment Zone Thickness from Lidar Backscatter Profiles, University of British Columbia, 2011 Ph.D. thesis.
[38] A.G. Straume, E.N. Koffi, K. Nodop, Dispersion modeling using ensemble forecasts compared to ETEX measurements, J. Appl. Meteorol. 37 (11) (1998) 1444–1456.
[39] G. Sugiyama, J.S. Nasstrom, Methods for Determining the Height of the Atmospheric Boundary Layer, Lawrence Livermore National Laboratory Internal Report UCRL-ID-133200 (1999).
[40] A. Von Engeln, J. Teixeira, A planetary boundary layer height climatology derived from ECMWF reanalysis data, J. Clim. 26 (17) (2013) 6575–6590.
[41] Y. Zhang, D.J. Seidel, S. Zhang, Trends in planetary boundary layer height over europe, J. Clim. 26 (24) (2013) 10071–10076.